Proceedings of the Design Society, Volume 5: ICED25
https://doi.org/10.1017/pds.2025.10074

Approach for a shape decomposition process to reduce material waste of structural sheet metal components

Lukas Kömm✉ and Kristin Paetzold-Byhain

TU Dresden, Germany

✉ lukas.koemm@tu-dresden.de

ABSTRACT: This work is driven by the aim to minimize material waste in the production of structural sheet metal components. Thus, a rule-based decomposition process for multiply connected planar shapes is presented, analyzing the shape's boundary and skeleton. Based on four cutting rules, shapes are decomposed to particularly extract straight and strut-like parts, allowing high packing densities for a reduction of material waste. Additionally, an alternative shape decomposition scenario is described, aiming for the avoidance of stress hotspots in structural components. In a case study with various shapes, effects on material waste are investigated involving a strip packing problem. Furthermore, effects on mechanical stress are analyzed. The results show potential to reduce material waste, but also disadvantages regarding mechanical stress. Aspects for further consideration are pointed out.

KEYWORDS: shape decomposition, sustainability, circular economy, ecodesign, design for x (DfX)

1. Introduction

Facing the ongoing climate change and the limited amount of raw materials, efforts need to be made to reduce material waste, including the production of sheet metal components. Structures built from sheet metal components are for example widely spread in the automotive industry (Mallick, 2021). The body-in-white of current passenger vehicles usually consists of visible outer panels, strongly influenced by design elements, and inner panels for reinforcement (Davies, 2012). Normally, the shape of the inner panel (Figure 1) is optimized to follow the load paths and therefore often shows holes or irregularly shaped cutouts (Mallick, 2021). On the one hand, a substantial amount of weight can be saved through this measure, reducing emissions during the vehicle's use-phase. On the other hand, a huge amount of material waste is produced when cutting irregular shapes from blanks. In this context, waste is defined as *"unwanted (. . .) material of any type, especially what is left after useful (. . .) parts have been removed"* based on the Cambridge Dictionary (Cambridge, 2014). According to Davies (2012) approx. 40 - 45% of the sheet metal required to build a car's body-in-white ends up as material waste in the press-shop.

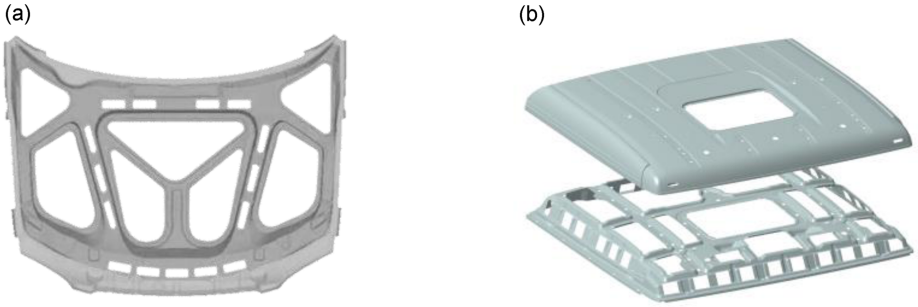

Figure 1. Inner panel of a car hood (a) (Yanping & Haijiang, 2010) and the outer and inner panel of a truck cabin roof (b)

The 12th of the 17 sustainable development goals of the United Nations (2015), in particular target 12.5, is claiming for a reduction of waste. Directive 2008/98/EC of the European Parliament (2008) presents a hierarchy on waste strategies: prevention, preparing for re-use, recycling, other (e.g. energy) recovery and disposal. Aiming for prevention as the most preferred strategy, this paper investigates shape decomposition to increase material efficiency. *"Shape decomposition is in general defined as complete partition of a single, connected region (shape) into disjunct sets of connected regions (parts)"* according to (Zeng et al., 2008, p. 682). It is hypothesized that decomposing shapes to extract approximately straight and strut-like parts, allows to pack parts densely on a blank and to reduce material waste.

2. State of the art

Most of the approaches that have been presented in the field of shape decomposition over the last decades are derived from psychological findings on humans' visual perception. Two rules are widely recognized: the *minima rule*, declaring that human perception prefers splitting shapes at the negative minima of curvature (Hoffman & Richards, 1984) and the *short cut rule*, *"(. . .) which states that human vision divides silhouettes into parts, using the shortest possible cuts"* (Singh et al., 1999, p. 637).
These rules form the baseline for many approaches, with some of them only analyzing the shape's boundary to position cuts (Latecki & Lakämper, 1999; Li et al., 2021) or others additionally incorporating the shape's skeleton into their analysis (Luo et al., 2015; Papanelopoulos & Avrithis, 2015; Papanelopoulos et al., 2019). The *combined skeleton-boundary approach* (Zeng et al., 2008) determines the so-called *protrusion strength* based on junction points of the skeleton and shows a high robustness against boundary noise. However, the calculation of the protrusion strength is only applicable to identify extremities of a shape, but not for the identification of straight and strut-like parts within a shape. Mi & DeCarlo (2007) calculate the so-called *relatability* by measuring the angle between the connecting line of two points on the boundary and their respective tangents. They mention, that their approach is not able to cut shallow necks, which are comparable to the desired straight parts.
Similarly, all the publications mentioned above consider only the decomposition of shapes with a single boundary and without holes - called *simply connected shapes* - cutting off extremities or other protruding areas. When defining a cut as a straight line that fully lies on the shape and does not intersect the boundary besides its two endpoints, a simply connected planar shape is decomposed into two disjunct parts for any randomly placed cut. In contrast, *multiply connected shapes* have more than one boundary due to holes or cutouts, like the body-in-white's inner panels. For multiply connected planar shapes, eventually more cuts need to be placed under consideration of the shapes connectivity to ensure disjunct parts, making the positioning of cuts more complex compared to simply connected shapes.
This limitation of many methods is also pointed out by G. Liu et al. (2014), proposing the *dual-space decomposition* for more complex and multiply connected shapes, which performs an optimization to select cuts. The *approximate convex decomposition* method (Lien & Amato, 2006) uses a dependency graph to incorporate the relations between the boundaries of multiply connected shapes and the *convex shape decomposition* by H. Liu et al. (2010) is based on the Morse theory. Also capable of decomposing multiply connected shapes is the *constraint morphological decomposition* (Kim et al., 2005), which in the first step cuts the shape recursively until no more parts can be split. As this process tends to over decomposition, parts are merged in a second step until a merging criterion - the difference in weighted convexity - is reached. The *feature-mapping* approach by Morin & Kim (2022) allows to decompose shapes into parts according to given dimensional restrictions, for example by a production machine, by optimizing the placement of partitioning profiles.
Some of these approaches generate results, that are getting close to the goal of extracting approximately straight parts. However, as none of the approaches is explicitly designed for the extraction of straight parts in the context of material waste reduction, it occurs that cuts are placed at sharp angles or in curved sections, which might cause protruding corners on the parts. This is disadvantageous for a dense packing of the parts and consequently for the amount of material waste.
Thus, a decomposition process for planar shapes is presented that explicitly extracts straight parts from multiply connected shapes in order to enable a dense packing. It is hypothesized that shape decomposition contributes to a reduction of material waste, but also tends to decrease the strength of structural components. Consequently, the decomposition process is extended by an alternative, stress-oriented scenario with effects on material waste and on mechanical stress being investigated.

3. Approach

First of all, a few terms are defined. The terminologies “shape”, “part” and “cut” are used according to the definitions in chapter 1. An “approximately straight and strut-like part” - also called “straight part” for convenience - defines in the context of this work a part, that has a significantly larger length than width, a low curvature along its length and a low increase or decrease in width along its length. Certain values for a significant length-width-ratio as well as tolerances are user-defined and adjustable.
The approach presented in this work describes a rule-based decomposition process utilizing the shape’s skeleton as well as its boundary. The main steps are: deriving and analyzing the skeleton, searching for possible candidate cuts, selecting the final cuts for decomposition and recombining parts.

3.1. Skeletonization

The geometry analysis for decomposing the shape is based on a skeleton approach for two reasons. The first one is to gain knowledge about the connectivity as a global shape property to ensure that cuts decompose a multiply connected shape into disjunct parts. The second reason for incorporating the skeleton is to find starting points for the cut search process. The skeleton curves are extracted by firstly rasterizing the shape with voxels, secondly applying a thinning algorithm (Lee et al., 1994) and finally fitting the chains to second-order B-splines (Denk et al., 2021). This approach has the advantage, besides low computational efforts, that rasterization reduces boundary noise. The skeleton’s connectivity is analyzed, differentiating between fully linked and open-ended skeleton curves (Figure 2a). To identify suitable starting points for the cut search process, the curvature of each skeleton curve is evaluated at equally spaced sample points with gap size g_{points}. The curvature plot is smoothed by calculating the moving average, involving an environment of five sample points before and ahead. Points of local minima in the moving average plot, considering a radius of three sample points, are selected as start points for the cut search process (Figure 2b).

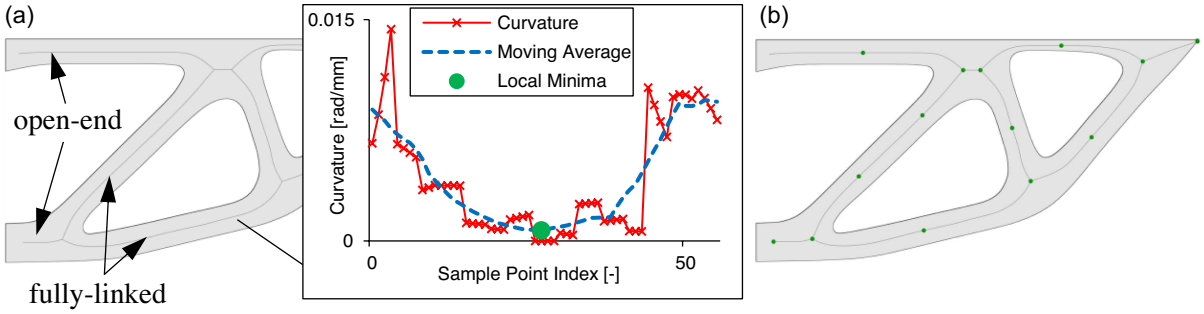

Figure 2. Shape with skeleton curves, curvature plot for a curve (a) and selected start points (b)

3.2. Cut search

The cut search process identifies possible candidate cuts for every skeleton curve based on local properties. The iterative process being executed for every determined start point is described in the following. From the first selected start point P, a line is drawn orthogonally to the corresponding skeleton curve with extend to the nearest boundary in each direction (Figure 3a). At both endpoints of this line the tangents t_1 and t_2 are formed to the corresponding contours. The angles α_1 and α_2 from the line to the tangents and the line’s length l are measured (Figure 3a) similar to the approach of Mi & DeCarlo (2007). Both angles are tested for the first cutting criterion with respect to a user-defined angular tolerance α_{Tol} (Equation 1). The set tolerance affects the allowed widening or tapering of a straight part.

$$|\alpha_1 - 90| \leq \alpha_{Tol} \wedge |\alpha_2 - 90| \leq \alpha_{Tol} \qquad \text{with} \qquad \alpha_1, \alpha_2, \alpha_{Tol} \text{ in } [°] \tag{1}$$

If the criterion is met, the line is added to a set of candidate cuts corresponding to the start point. The next sample point on that skeleton curve is picked repeating the same process, but additionally applying a second criterion (Equation 2) comparing the length l of the newly drawn line to the length of the previous line $l_{previous}$ (Figure 3b). This second criterion applies to all lines besides those at a start point.

$$|l - l_{previous}| \leq \Delta l_{Tol} = g_{points} * 2\tan(\alpha_{Tol}) \tag{2}$$

If both criteria are met, the line is also added to the set of candidate cuts corresponding to the start point from which ongoing the line was identified. This process is iteratively repeated in one direction along the

curve, continuously adding candidate cuts until a cutting criterion is not satisfied or the last sample point on the skeleton curve is reached. Next, the iterative process is repeated along the opposite direction of the skeleton curve, adding further candidate cuts to the set (Figure 3c).

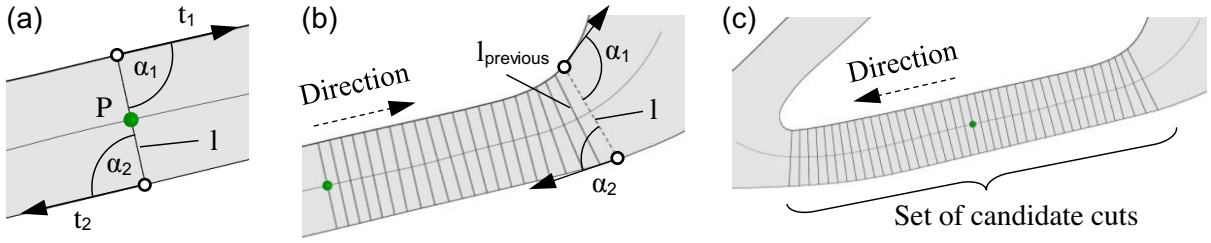

Figure 3. Tangents at orthogonally drawn line (a), iterations along first direction (b) and repetition in the opposite direction to build a set of candidate cuts (c)

The set is closed with the end of the iterative process along the opposite direction. The whole process is then repeated for all identified start points (Figure 4). Finally, overlapping sets of candidate cuts are merged to one set (Figure 5a). In cases where no candidate cut has been found for a skeleton curve, the shortest drawn line corresponding to that skeleton curve is picked without respect to both criteria to maintain a decomposition into disjunct parts. For every set, the set's length l_{set} based on the number of cuts $n_{cut,set}$ and its average width w_{set} are calculated to be tested for the third criterion (Equation 3).

$$\frac{l_{set}}{w_{set}} \geq r_{lw} \quad \text{with} \quad l_{set} = (n_{cuts,set} - 1) * g_{points} \quad \text{and} \quad w_{set} = \frac{1}{n_{cuts,set}} \sum_{i=1}^{n_{cuts,set}} l_{cut,i} \tag{3}$$

All sets satisfying this criterion for a desired length-width-ratio r_{lw} are classified as "straight".

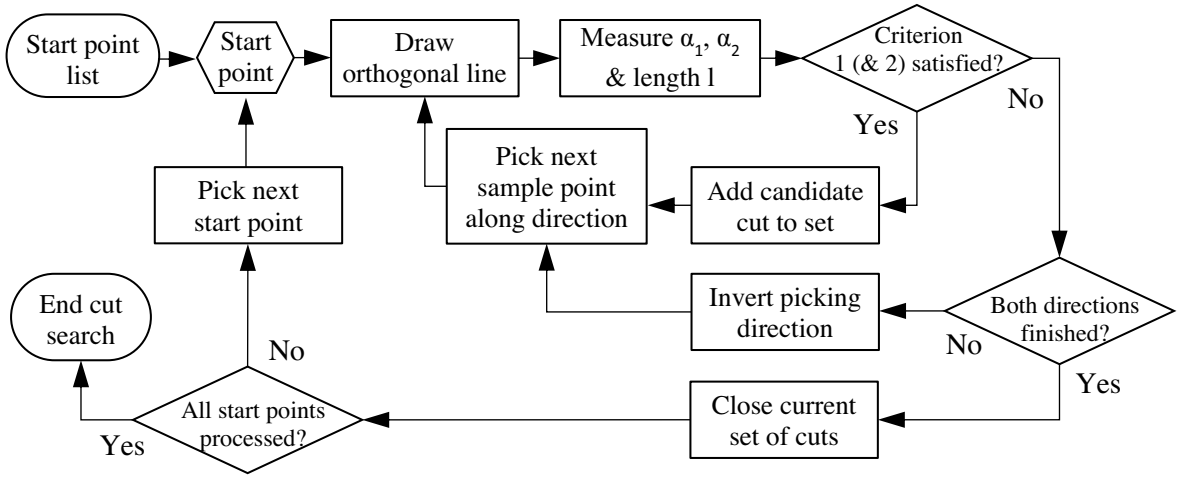

Figure 4. Block diagram of the iterative cut search process

3.3. Cut selection

After all possible candidate cuts have been identified, those which shall be finally used for the decomposition are selected. Two different scenarios are described in the following.

Scenario A focuses entirely on a dense packing by extracting straight parts, while alternatively, scenario B aims to include aspects regarding mechanical stress as well. In the context of structural components, it needs to be considered that joints, like for example weld seams or spot welds, that are required to join decomposed parts later in the manufacturing process, usually have a lower strength compared to the unaffected base material. At the same time, stress hotspots within a structural component often occur in corners or areas with strongly curved boundaries. Consequently, it is hypothesized that for a cut selection that favors mechanical stress, joints or cuts respectively should not be positioned in these areas. Thus, they are shifted to the middle of straight sections in scenario B.

For the selection of final cuts, each set of candidate cuts - obtained based on local properties during the cut search process - is combined with the global information about the connectivity of the

corresponding skeleton curve. To extract straight parts for scenario A while ensuring a decomposition into disjunct parts, but also to avoid unnecessary cuts, cutting rules for four different cases are defined (Table 1; Figure 5a). One of the four cutting rules is applied on each set of candidate cuts.

Table 1. Four cutting rules to extract straight parts

Case	Set classification	Skeleton curve connectivity	Action
1	straight	fully-linked	2 cuts
2	straight	open-end	1 cut
3	not straight	fully-linked	1 cut
4	not straight	open-end	No cut

In case number 1, the first and last candidate cut of the set are selected for the decomposition. Each pair of cuts in case 1 extracts a straight part from the shape. In case number 2, only one cut is required to achieve a disjunct straight part. Therefore, the candidate cut furthest away from the open-end point is selected. In case 3, according to the shortcut rule, the shortest candidate cut of the set is selected. And in case 4 no action is required and no cut will be selected. The selected cuts are shown in Figure 5b. If selected cuts exceptionally intersect, the longer cutting line is trimmed on the shorter one.
Scenario B can be easily derived from scenario A, with cutting rules 3 & 4 remaining unchanged. The rules for case 1 & 2 are slightly modified by selecting one cut in the middle of the set instead. This minor change maintains a decomposition into disjunct parts while shifting cutting lines into the middle of straight parts (Figure 5c).

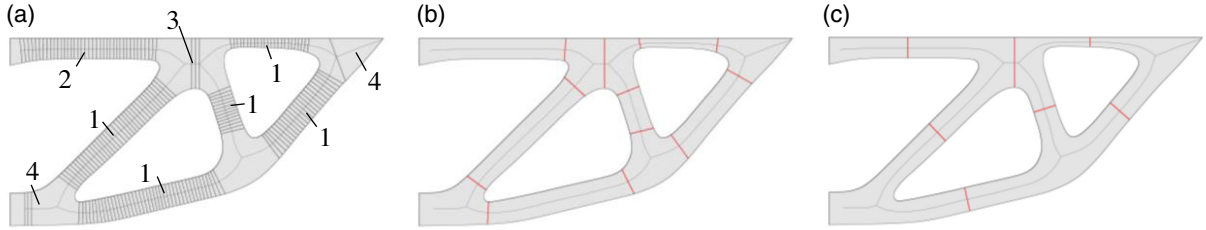

Figure 5. Sets of candidate cuts with case numbers for every skeleton curve (a), final cuts in red for scenario A (b) and for scenario B (c)

3.4. Part recombination

As especially Scenario A tends to over-decomposition resulting in many relatively small parts, those are recombined in a final step similar to Kim et al. (2005). Recombination is performed in an iterative and greedy manner starting from the part with the smallest surface area. The first part and its adjacent neighbors are picked and their surface areas A_{Part} as well as the areas of their individual convex hulls A_{Hull} are determined (Figure 6a). As a measure for concavity c the ratio between the part's and the hull's surface area is calculated according to Equation 4.

$$c = \frac{A_{Part}}{A_{Hull}} \tag{4}$$

The part is then merged with each of its neighbors for which new convex hulls are created (Figure 6b) and areas A^*_{Part} and A^*_{Hull} measured. For those the new concavity c* is calculated as well following Equation 4. To decide whether to keep one of the merging options, for each the weighted difference in concavity Δc with regard to the original parts is calculated (Equation 5). Weights are defined based on surface areas.

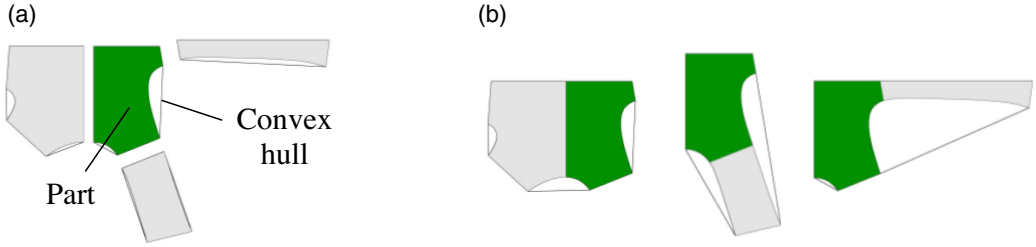

Figure 6. Part and its neighbors with individual convex hulls (a) and merging options (b)

$$\Delta c = \frac{A_{Ppart,1}}{A^*_{Part}} * (c_1 - c^*) + \frac{A_{Part,2}}{A^*_{Part}} * (c_2 - c^*) \quad (5)$$

The merging option with the lowest Δc below the desired threshold is kept. The iterative process stops as soon as no further merging operations within the threshold are possible.

4. Case study

To validate the presented process and to investigate the effects of decomposed shapes on the material waste of sheet metal components as well as on stress hotspots, a case study is conducted. Therefore, the proposed process is applied on various multiply connected planar shapes, including shapes generated by topology optimization, shapes based on other publications and the shape of the inner panel of the truck cabin roof presented in the first chapter. The latter was flattened to a planar shape before and small holes were removed for simplicity.

4.1. Decomposition

Table 2 gives an overview about the settings used for the tolerances and thresholds α_{Tol}, r_{lw} and Δc in this case study as well as the numbers of parts n_{Parts} obtained by scenario A and B for the various shapes. Scenario A generates mostly a higher number of parts compared to scenario B - even up to twice as many for a few shapes - due to the extraction of straight parts, which leaves connecting parts in between.

Table 2. Settings for decomposition and results

Shape	Topo1	Topo2	Topo3	Topo4	Roof	Circle	Square	Spike	Spatula	Car
Figure	7(a)	7(b)	7(c)	7(d)	7(e)	8(a)	8(b)	8(c)	8(d)	8(e)
α_{Tol}					15°					10°
r_{lw}					1.5					1.0
Δc_A		0.15			0.10			0.07		
$n_{Parts,A}$	14	18	5	11	37	4	4	4	7	8
Δc_B					0.07					
$n_{Parts,B}$	7	10	5	10	30	2	4	2	5	4

Graphical representations of the results for the topology optimized shapes as well as the inner panel of the cabin roof are shown in Figure 7. For scenario A, the extracted straight parts are clearly recognizable.

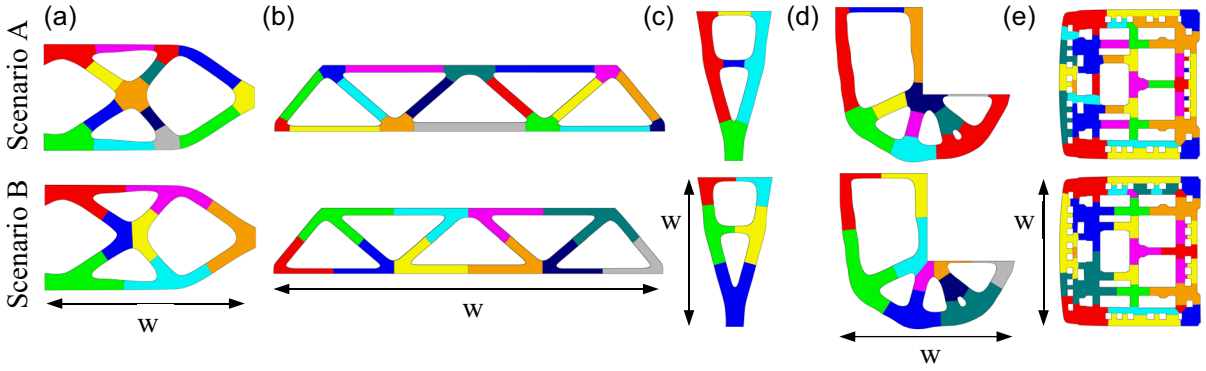

Figure 7. Results for topology optimized shapes based on Bendsøe & Sigmund (2004) (a)-(b), inspired by or based on Duriez et al. (2022) (c)-(d) and the inner panel of the cabin roof (e)

Only the inner panel of the cabin roof as the most complex part in this study shows a few irregularities. To demonstrate the robustness of the presented process and that it is not limited to the application on topology optimized or other structural components, it is applied on some shapes based on other publications. Results from these publications are qualitatively compared to those generated by the own process, proving that straight parts are identified properly for these kind of shapes as well (Figure 8).

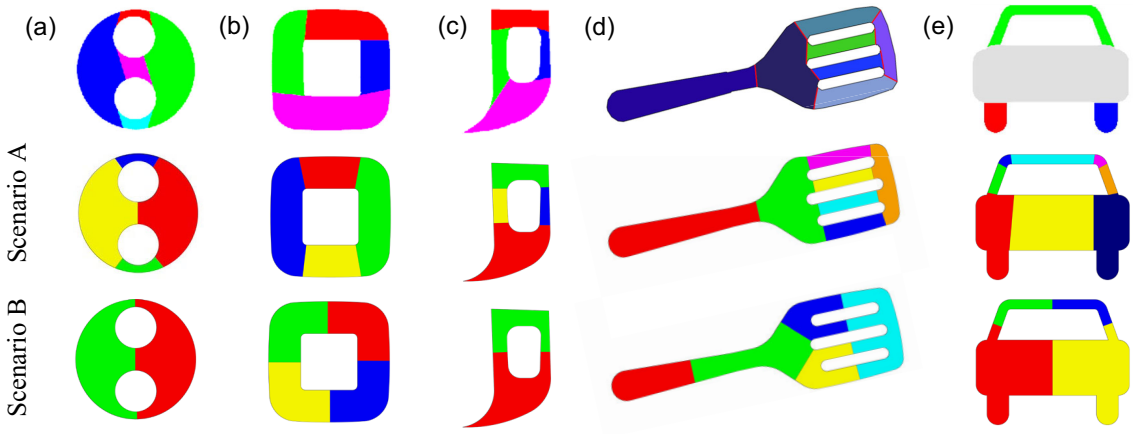

Figure 8. Results from H. Liu et al. (2010) (a)-(c), G. Liu et al. (2014) (d) and Kim et al. (2005) (e) in the first row compared to results from scenario A and B of the own process

4.2. Effect on material waste

According to the motivation of this work, the effect of shape decomposition on material waste is investigated for the five shapes shown in Figure 7. Therefore the following example considers a strip packing problem for every individual shape with a blank of width w, matching the shape's largest dimension (Figure 7). On this blank n pieces of a shape, in this example for n = 4, are to be placed in a way to minimize length l. Same applies for the parts in which the shapes were decomposed in scenario A and scenario B. Shapes and parts are arranged on the blank with no spacing in between. For this example, the packing was performed manually as the selection of a suitable algorithm should not be the focus of this work and to not affect the result by an algorithm's performance. The length l of the strip required to arrange all four shapes or the corresponding parts is measured and the material efficiency η_{Mat} is calculated (Table 3) according to Equation 6.

$$\eta_{Mat} = \frac{n * A_{Shape}}{l * w} \tag{6}$$

Table 3. Results of the strip packing problem

Shape	Topo1		Topo2		Topo3		Topo4		Roof	
	Length	η_{Mat}	Length	η_{Mat}	Length	η_{Mat}	Length	η_{Mat}	Length	η_{Mat}
Unsplit	1.84w	40.0%	0.67w	34.8%	1.49w	50.0%	2.54w	42.9%	3.74w	61.2%
Scenario A	0.92w	80.2%	0.27w	85.6%	1.03w	72.3%	1.39w	78.2%	2.88w	79.3%
Scenario B	1.18w	62.0%	0.42w	55.4%	1.09w	68.7%	1.49w	73.1%	3.02w	75.9%

4.3. Effect on mechanical stress

Effects on mechanical stress in the context of structural components are analyzed for the four topology-optimized shapes. For this example, due to the extensive range of materials and joining techniques, a case is selected with structural components being manufactured from steel grade S460M and joined by butt welds. All parts - for scenario A and B - have the identical uniform thickness like the corresponding unsplit shape. A finite-element simulation with OptiStruct is conducted, using a linear-elastic material model and applying the linear static loads on the structures for which they have been optimized. Quad-dominant meshes with second order elements and sizes defined on basis of mesh convergence studies are used. For comparability, the identical mesh is used for the unsplit shape and for scenarios A and B.
In accordance with standard DIN EN 1993-1-8, the allowed stress limit for butt welds with complete joint penetration can be assumed equal to the stress limit of the weaker part, when utilizing a proper filler material. For the prevailing case with identical material and thicknesses, this means there are no downsides compared to an unsplit and unwelded structure. Instead, a less favorable case is chosen for this example considering a butt weld with only a partial joint penetration, for which Equation 7 is used to calculate the allowed weld seam stress following DIN EN 1993-1-8 (DIN, 2010).

$$\sigma_{limit,weld} = \frac{R_m}{\sqrt{3} * \beta_w * \gamma_{M2}} \tag{7}$$

This results in a stress limit of $\sigma_{limit,weld}$ = 249 MPa for weld seams, plugging in an ultimate strength of R_m = 540 MPa based on DIN EN 10025-4 and a correlation factor β_W = 1.0 as well as a partial safety factor for joints γ_{M2} = 1.25 according to DIN EN 1993-1-8. The utilization factor UF, the reciprocal of the safety factor S, is calculated for every finite-element by dividing its von Mises stress σ_{vMises} by the corresponding stress limit σ_{limit} (Equation 8).

$$UF = \frac{\sigma_{vMises}}{\sigma_{limit}} = \frac{1}{S} \tag{8}$$

UF is calculated for elements directly adjacent to a weld line with $\sigma_{limit} = \sigma_{limit,weld}$ and for elements in the remaining unaffected areas with $\sigma_{limit} = R_e$ = 460 MPa. For a better comparability UF values are scaled, so the maximum value for the unsplit shape is 1.0, suggesting it is dimensioned for the maximum stress and showing the increase for the decomposed shapes by the displayed factors (Figure 9).

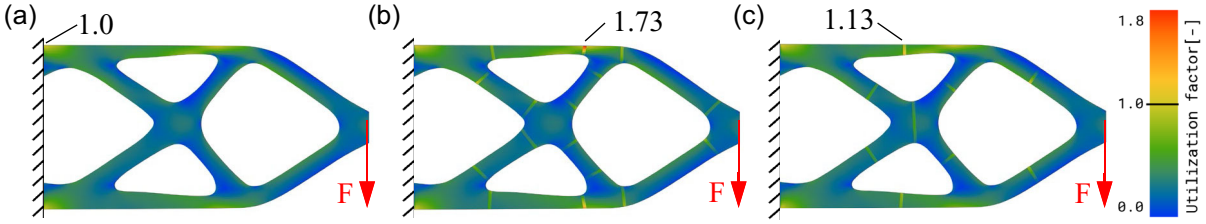

Figure 9. Plots of utilization factor UF for shape "Topo1" with maxima of UF marked for the unsplit shape (a), scenario A (b) and scenario B (c)

In Table 4 the results for all four analyzed shapes are listed. It includes the maximum UF as well as the amount of critical weld seams - with an UF larger 1.0 - out of the total number of weld seams (w_{crit} / Σ).

Table 4. Results of the structural analysis

Shape	Topo1		Topo2		Topo3		Topo4	
	max. UF	w_{crit} / Σ	max. UF	w_{crit} / Σ	max. UF	w_{crit} / Σ	max. UF	w_{crit} / Σ
Unsplit	1.0	-	1.0	-	1.0	-	1.0	-
Scenario A	1.73	2 / 16	1.0	0 / 22	1.38	2 / 6	1.33	3 / 15
Scenario B	1.13	1 / 9	1.23	1 / 14	1.44	4 / 6	1.84	2 / 14

5. Discussion

The proposed process has shown itself to be reliable in extracting straight parts from multiply connected shapes while ensuring a full decomposition into disjunct parts by applying the four defined cutting rules. It is applicable to different types of shapes with no or very little fine-tuning of the parameters α_{Tol} and r_{lw} and also proves robust to low frequency boundary noise, like in case of shape "Topo4" (Figure 7d).
The comparison with the results of other publications shows advantages regarding the positioning of cuts, but also potential for further improvements. Particularly, the decomposed "Spatula" shape of scenario A shows very accurately positioned cuts, causing no sharp or protruding corners on the parts, compared to the other paper's result. However, the decomposed "Car" shape of scenario A shows small protruding corners at the transition to the window frame, indicating that cuts being placed strictly orthogonal to the skeleton curve are not ideal in every case. Thus, the orientation of the cuts should be made adjustable to the surrounding boundaries.
The approach of firstly rather over-decomposing the shape - mainly in scenario A - and later recombining the parts is on the one hand a safety mechanism to ensure fully disjunct parts and on the other hand offers a high degree of freedom in recombining parts. Besides the shown approach using a given threshold for Δc as a merging criterion, it is also conceivable to merge parts until a desired number of parts or a dimensional limit is reached. During the case study, part recombination has been found sensitive to the parts surface areas and their original concavity, requiring minor adjustments to Δc. For the most complex

part of the case study, the inner panel of the cabin roof, some irregularly merged parts are visible caused by the greedy merging behavior, showing potential for future improvements.
Focusing on the effects of shape decomposition, the case study clearly shows an increase in material efficiency and a reduction of material waste for both scenarios, with scenario A consistently outperforming scenario B. Taking into account the five investigated shapes, scenario A allows to reduce the amount of material waste by 59 - 91%, on average by 75%. In comparison, scenario B reduces the material waste by 50 - 72% and on average by 59% as these parts tend to have larger concavities compared to parts from scenario A, resulting in a less dense packing. The difference between both scenarios gets larger for more strut-like shapes. These results confirm the hypothesis that shape decomposition leads to a reduction of material waste, especially when extracting straight parts.
However, in a manufacturing context, it needs to be considered that the example presented in chapter 4.2 mainly applies to a laser cutting process. In case of other processes like stamping, parts have to be arranged with larger gaps in between, which can be more disadvantageous for many small parts. Similar factors must be taken into account in case of downstream processes such as deep drawing or spot welding that require additional margin or overlaps on the parts. More case-specific investigations are needed including a life cycle assessment with a wider scope that also covers environmental effects, for example caused by the energy demand of joining processes or by a larger number of stamping tools.
Regarding the effect on mechanical stress, the case study shows disadvantages compared to an unsplit shape in most of the cases, but no clear tendency comparing scenario A and B. Contrary to the hypothesis scenario A outperforms scenario B in some cases, in terms of the maximum UF as well as the number of critical weld seams. This suggests that an ideal positioning of cuts with regard to the avoidance of stress hotspots cannot be linked to a certain scenario, but depends on the individual shape and load paths. The impact on mechanical stress is also affected by the joint selection, as pointed out in chapter 4.3.
On the one hand, shape decomposition tends to have negative effects on mechanical stress, whose compensation with thicker sheet metals, for example, counteracts the reduction of material waste. On the other hand, it should be taken into account that decomposed shapes allow to vary the thickness for every part individually or to use different material grades. This improves the adjustability to local stress hotspots and can enable a reduction of the components weight and of input material, leading to an optimization problem which will be investigated in future work.
Another aspect that has not been considered in this work is the economic one. While a reduction of material waste achieved by shape decomposition leads to savings in material costs, costs for manufacturing tend to increase due to additional joining processes, the handling of multiple parts or an increased number of tools, as in the case of stamping. Finally, the overall profitability weighted against environmental benefits will decide on the likelihood of an industrial application of one of the scenarios.

6. Conclusion

In this paper a process for the decomposition of multiply connected planar shapes was proposed that focuses in particular on the extraction of straight, strut-like parts. Cutting rules for two differently motivated scenarios, with scenario A aiming for a dense packing and scenario B for the avoidance of stress hotspots, have been defined. In a case study, the process is applied on various shapes and effects on material waste and mechanical stress in the context of structural components are investigated. For the considered example, a significant reduction of material waste is achieved for both cutting scenarios, while there are disadvantages regarding mechanical stress. Finally, further aspects that should be taken into account in the context of an application on structural sheet metal components are pointed out.

Acknowledgement

The author thanks the industry partner MAN Truck & Bus SE for funding this research project. Statements and information in this paper do not necessarily represent the opinion of MAN Truck & Bus.

References

Bendsøe, M. P., & Sigmund, O. (2004). *Topology optimization: Theory, methods, and applications* (2. ed., corrected printing). Springer. https://doi.org/10.1007/978-3-662-05086-6

Cambridge University Press & Assessment. (2014). *Waste*. Cambridge Dictionary. https://dictionary.cambridge.org/de/worterbuch/englisch/waste

Davies, G. (2012). Materials for automobile bodies (2nd ed.). Butterworth-Heinemann. http://www.sciencedirect.com/science/book/9780080969794
Denk, M., Rother, K., & Paetzold, K. (2021). Subdivision surface mid-surface reconstruction of topology optimization results and thin-walled shapes using surface skeletons. *Proceedings of the Design Society*, 1, 2771–2780. https://doi.org/10.1017/pds.2021.538
DIN German Institute for Standardization. (2010). Eurocode 3: Design of steel structures - Part 1-8: Design of joints (DIN EN 1993-1-8:2010-12). DIN Media GmbH.
Duriez, E., Morlier, J., Azzaro-Pantel, C., & Charlotte, M. (2022). Ecodesign with topology optimization. *Procedia CIRP*, 109, 454–459. https://doi.org/10.1016/j.procir.2022.05.278
European Parliament and Council of the European Union. (2008). Directive 2008/98/EC of the European Parliament and of the Council of 19 November 2008 on waste and repealing certain Directives. *Official Journal of the European Union.* https://eur-lex.europa.eu/eli/dir/2008/98/oj
Hoffman, D. D., & Richards, W. A. (1984). Parts of recognition. *Cognition*, 18(1-3), 65–96. https://doi.org/10.1016/0010-0277(84)90022-2
Kim, D. H., Yun, I. D., & Lee, S. U. (2005). A new shape decomposition scheme for graph-based representation. *Pattern Recognition*, 38(5), 673–689. https://doi.org/10.1016/j.patcog.2004.10.003
Latecki, L. J., & Lakämper, R. (1999). Convexity Rule for Shape Decomposition Based on Discrete Contour Evolution. *Computer Vision and Image Understanding*, 73(3), 441–454. https://doi.org/10.1006/cviu.1998.0738
Lee, T. C., Kashyap, R. L., & Chu, C. N. (1994). Building Skeleton Models via 3-D Medial Surface Axis Thinning Algorithms. *CVGIP: Graphical Models and Image Processing*, 56(6), 462–478. https://doi.org/10.1006/cgip.1994.1042
Li, Z., Qu, W., Qi, H., & Stojmenovic, M. (2021). Near-convex decomposition of 2D shape using visibility range. *Computer Vision and Image Understanding*, 210, 103243. https://doi.org/10.1016/j.cviu.2021.103243
Lien, J.-M., & Amato, N. M. (2006). Approximate convex decomposition of polygons. *Computational Geometry*, 35(1-2), 100–123. https://doi.org/10.1016/j.comgeo.2005.10.005
Liu, G., Xi, Z., & Lien, J.-M. (2014). Dual-Space Decomposition of 2D Complex Shapes. In *2014 IEEE Conference on Computer Vision and Pattern Recognition* (pp. 4154–4161). IEEE. https://doi.org/10.1109/CVPR.2014.529
Liu, H., Liu, W., & Latecki, L. J. (2010). Convex shape decomposition. In *2010 IEEE Computer Society Conference on Computer Vision and Pattern Recognition* (pp. 97–104). IEEE. https://doi.org/10.1109/CVPR.2010.5540225
Luo, L., Shen, C., Liu, X., & Zhang, C. (2015). A computational model of the short-cut rule for 2D shape decomposition. *IEEE Transactions on Image Processing: A Publication of the IEEE Signal Processing Society*, 24(1), 273–283. https://doi.org/10.1109/TIP.2014.2376188
Mallick, P. K. (2021). Designing lightweight vehicle body. In *Materials, Design and Manufacturing for Lightweight Vehicles* (pp. 405–432). Elsevier. https://doi.org/10.1016/B978-0-12-818712-8.00010-0
Mi, X., & DeCarlo, D. (2007). Separating Parts from 2D Shapes using Relatability. In *2007 IEEE 11th International Conference on Computer Vision* (pp. 1–8). IEEE. https://doi.org/10.1109/ICCV.2007.4409014
Morin, R., & Kim, I. Y. (2022). Partitioning a topology-optimized structure into additively manufacturable parts using a feature-mapping approach: a novel decomposition optimization method. *Structural and Multidisciplinary Optimization*, 65(10). https://doi.org/10.1007/s00158-022-03394-8
Papanelopoulos, N., & Avrithis, Y. (2015). Planar shape decomposition made simple. In X. Xie, M. W. Jones, & G. K. L. Tam (Eds.), *Proceedings of the British Machine Vision Conference 2015* (13.1–13.12). British Machine Vision Association. https://doi.org/10.5244/C.29.13
Papanelopoulos, N., Avrithis, Y., & Kollias, S. (2019). Revisiting the medial axis for planar shape decomposition. *Computer Vision and Image Understanding*, 179, 66–78. https://doi.org/10.1016/j.cviu.2018.10.007
Singh, M., Seyranian, G. D., & Hoffman, D. D. (1999). Parsing silhouettes: The short-cut rule. *Perception & Psychophysics*, 61(4), 636–660. https://doi.org/10.3758/BF03205536
United Nations. (2015). *Transforming our world: the 2030 Agenda for Sustainable Development (A/RES/70/1).* https://documents.un.org/doc/undoc/gen/n15/291/89/pdf/n1529189.pdf
Yanping, L., & Haijiang, L. (2010). Material and Structural Optimization for Engine Hood Inner Panel of Car Body Aimed to Lightweight. In *2010 WASE International Conference on Information Engineering* (pp. 291–294). IEEE. https://doi.org/10.1109/ICIE.2010.360
Zeng, J., Lakaemper, R., Yang, X., & Li, X. (2008). 2D Shape Decomposition Based on Combined Skeleton-Boundary Features. In G. Bebis, R. Boyle, B. Parvin, D. Koracin, P. Remagnino, F. Porikli, J. Peters, J. Klosowski, L. Arns, Y. K. Chun, T.-M. Rhyne, & L. Monroe (Eds.), *Lecture Notes in Computer Science. Advances in Visual Computing* (Vol. 5359, pp. 682–691). Springer Berlin Heidelberg. https://doi.org/10.1007/978-3-540-89646-3_67